CHAPTER 5

# ANALYSIS OF HEAT TRANSFER PERFORMANCE OF TWO DIMENSIONAL NANOFLUID FLOW IN PRESENCE OF MAGNETIC FIELD

Content of this chapter is communicated.

# Chapter 5

## ANALYSIS OF HEAT TRANSFER PERFORMANCE OF TWO DIMENSIONAL NANOFLUID FLOW IN PRESENCE OF MAGNETIC FIELD

One dimensional MHD nanofluid problems discussed so far are of much importance as analytical solutions can be obtained, and may find applications in many industrial and engineering problems which can be treated as one dimensional fluid flow. But, there are many practical problems which cannot be solved efficiently using one dimensional modelling and thus need arises for considering higher dimensions. This chapter deals with two dimensional nanofluid flow in presence of magnetic field. Extension of work discussed in previous chapters to two dimensional models, results in more complicated and nonlinear system of partial differential equations. So analytical methods like Laplace transform technique are not adequate, and system need to be solved using semi analytical or numerical methods.

## 5.1 Introduction

Many industrial processes such as moving pistons, hydrodynamical machines, polymer processing, food processing, loading of machine components, lubrication and the squeezed film in power transmission require thorough knowledge of squeezing unsteady nanofluid flow through parallel plates. Sheikholeslami et. al. [71] discussed the unsteady squeezing nanofluid flow and heat transfer. Sheikholeslami and Ganji [75] applied HPM to solve the problem of heat transfer in the unsteady squeezing nanofluid flow between parallel plates. The squeezing MHD flow of nanofluid between two parallel plates, is studied by Acharya et al. [2]. Madaki et al. [41] investigated effects of thermal radiation and heat generation/absorption on squeezing unsteady nanofluid flow. Additional information regarding effects of heat generation or absorption is vital in cooling processes as reflected in work done by Alsaedi et al. [5].

## 5.2 Novelty of the Problem

The intention of this study is to examine influence of the thermal radiation on nanofluid flow through squeezing parallel plates. Effects of thermal interfacial resistance and Brownian motion on thermal conductivity are often ignored. Novelty of the present work is the inclusion of above phenomenon along with micro mixing in suspensions. The simplified system of ODE is solved using the HAM. The effects of the relevant parameters are discussed.

## 5.3 Mathematical Formulation of the Problem

Fluid considered in this study is $Al_2O_3$ − water nanofluid. Squeezing flow is assumed to be between two horizontal parallel plates situated at $l(t) = L(1 - at)^{1/2}$ units apart. Here L is the original position of the plate, $a > 0$ signifies that plates are squeezed until they touch each other at $t = \frac{1}{a}$ and plates moves in opposite direction for $a < 0$. A coordinate system is considered as displayed in Figure 5.1. A uniform magnetic flux with density ($B$ is the initial value) $B(t) = B/\sqrt{1 - at}$ is applied.

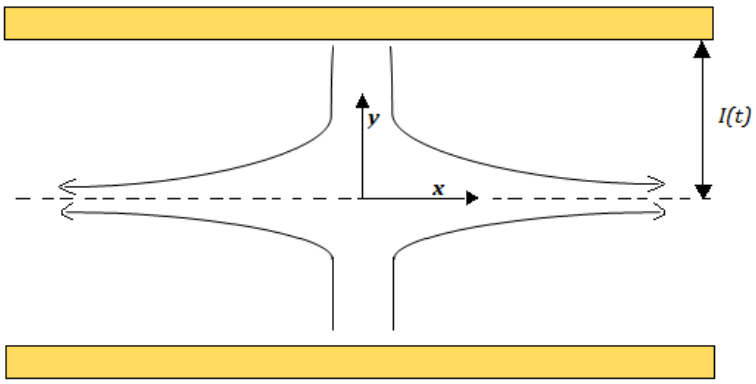


**Figure 5.1**: Physical Sketch of the Problem

Under above assumptions, governing equations are:

$$\frac{\partial u}{\partial x} + \frac{\partial v}{\partial y} = 0 \qquad (5.1)$$

$$\rho_{nf}\left(\frac{\partial u}{\partial t}+u\frac{\partial u}{\partial x}+v\frac{\partial u}{\partial y}\right)=\mu_{nf}\left(\frac{\partial^2 u}{\partial x^2}+\frac{\partial^2 u}{\partial y^2}\right)-\sigma_{nf}B^2(t)u \tag{5.2}$$

$$\rho_{nf}\left(\frac{\partial v}{\partial t}+u\frac{\partial v}{\partial x}+v\frac{\partial v}{\partial y}\right)=\mu_{nf}\left(\frac{\partial^2 v}{\partial x^2}+\frac{\partial^2 v}{\partial y^2}\right) \tag{5.3}$$

$$\left(\rho c_p\right)_{nf}\left(\frac{\partial T}{\partial t}+u\frac{\partial T}{\partial x}+v\frac{\partial T}{\partial y}\right)=k_{nf}\left(\frac{\partial^2 T}{\partial x^2}+\frac{\partial^2 T}{\partial y^2}\right)+\mu_{nf}\left(2\left[\left(\frac{\partial u}{\partial x}\right)^2+\left(\frac{\partial v}{\partial y}\right)^2\right]+\left(\frac{\partial u}{\partial y}+\frac{\partial v}{\partial x}\right)^2\right)$$

$$-\frac{\partial q_r}{\partial y}+\frac{\left(\rho c_p\right)_{nf}Q(T-T_0)}{\rho_{nf}} \tag{5.4}$$

where

$$\rho_{nf}=(1-\emptyset)\rho_f+\emptyset\rho_s \tag{5.5}$$

$$\sigma_{nf}=\sigma_f[1+\frac{3(\sigma-1)\emptyset}{(\sigma+2)-(\sigma-1)\emptyset}],\sigma=\frac{\sigma_s}{\sigma_f} \tag{5.6}$$

$$\left(\rho c_p\right)_{nf}=(1-\emptyset)(\rho c_p)_f+\emptyset(\rho c_p)_s \tag{5.7}$$

$$k_{nf}=k_f\left[1-3\frac{\emptyset(k_f-k_s)}{2k_f+k_s+\emptyset(k_f-k_s)}\right] \tag{5.8}$$

Considering micro mixing in suspensions,

$$\mu_{nf}=\mu_{static}+\mu_{Brownian}=\frac{\mu_f}{(1-\emptyset)^{2.5}}+\frac{k_{Brownian}*\mu_f}{k_f*Pr_f} \tag{5.9}$$

$q_r$ becomes [61],

$$q_r=-\frac{4\sigma^*}{3k^*}\frac{\partial T^4}{\partial y}=-\frac{4\sigma^*}{3k^*}\frac{\partial(4T_0{}^3T-3T_0{}^4)}{\partial y} \tag{5.10}$$

The thermo-physical properties are as in Table 1.1.

Boundary conditions are

$$u=0;\ v=\frac{dl}{dt};\ T=T_L\ at\ y=l(t) \tag{5.11}$$

$$u=0;\ v=0;\ \frac{\partial T}{\partial y}=0\ at\ y=0 \tag{5.12}$$

Introducing non dimensional variables

$$\eta = \frac{y}{L(1-at)^{1/2}},\ u = \frac{ax}{2(1-at)} f'(\eta), v = \frac{-aL}{(1-at)^{1/2}} f(\eta),\ \theta(\eta) = \frac{T}{T_L},\ B(t) = \frac{B}{(1-at)^{1/2}},\ \delta = \frac{L}{x},$$

$$\lambda = \frac{Q2L(T_w - T_0)(1-at)}{k_f T_w \rho_f} \tag{5.13}$$

Therefore, the equations reduce to:

$$a_1 f^{iv} - S(f'f'' + (-f+\eta)f''' + 3f'') - a_3 M^2 f'' = 0 \tag{5.14}$$

$$\theta'' + Pr\left(Sa_2(f-\eta)\theta' + Eca_4(4\delta^2 f'^2 + f''^2)\right) + a_2\theta\lambda = 0 \tag{5.15}$$

where

$$Pr = \frac{\mu_f (\rho c_p)_f}{\rho_f k_f},\ M = \frac{\sigma_f a B^2 L^2}{\rho_f v_f},\ S = \frac{aL^2}{2v_f},\ Ec = \frac{\rho_f (ax)^2}{(\rho c_p)_f T_L 4(1-at)^2} \tag{5.16}$$

$$b_0 = 1 - \emptyset \tag{5.17}$$

$$b_1 = (b_0 + \emptyset \frac{\rho_s}{\rho_f}), \tag{5.18}$$

$$b_2 = \frac{1}{{b_0}^{2.5}} \tag{5.19}$$

$$b_3 = (b_0 + \emptyset \frac{(\rho c_p)_s}{(\rho c_p)_f}), \tag{5.20}$$

$$b_4 = \frac{k_{nf}}{k_f}, \tag{5.21}$$

$$b_5 = \frac{\sigma_{nf}}{\sigma_f}, \tag{5.22}$$

$$a_1 = \frac{1}{{b_0}^{2.5} b_1}, \tag{5.23}$$

$$a_2 = \frac{b_3}{b_4 + Nr}, \tag{5.24}$$

$$a_3 = \frac{b_5}{b_1}, \tag{5.25}$$

$$a_4 = \frac{b_2}{b_4}, \tag{5.26}$$

$$Nr = \frac{16\sigma^* {T_0}^3}{3k^* k_f} \tag{5.27}$$

subject to

$$f = 0, f'' = 0,\ \theta' = 0\ at\ \eta = 0 \tag{5.28}$$

$$f = 1, f' = 0,\ \theta = 1\ at\ \eta = 1 \tag{5.29}$$

## 5.4 Solution by Homotopy analysis Method

Equations (5.14) – (5.15) are coupled non-linear ordinary differential equations whose exact solutions may not be possible. To solve these equations together with the boundary conditions (5.28) – (5.29), the homotopy analysis method (HAM) developed by Liao [40] is employed.

Initial guess:

$$f_0(\eta) = (3\eta - \eta^3)/2; \theta_0(\eta) = 1; \tag{5.30}$$

with linear operators:

$$L_f = \frac{\partial^4 f}{\partial \eta^4}\ ,\ L_\theta = \frac{\partial^2 \theta}{\partial \eta^2} \tag{5.31}$$

such that

$$L_f(C_1 + C_2\,\eta + C_3\eta^2 + C_4\eta^3) = 0,\ L_\theta(\,C_5 + C_6\eta) = 0. \tag{5.32}$$

where $c_1,\ \ c_2, \ldots, c_6$ are constants.

The zeroth order deformation problems are constructed as follows:

$$(1-p)L_f\left[\hat{f}(\eta;\ p) - f_0(\eta)\right] = p\hbar_f N_f\left[\hat{f}(\eta;\ p), \hat{\theta}(\eta;\ p)\right], \tag{5.33}$$

$$(1-p)L_\theta\left[\hat{\theta}(\eta;\ p)-\theta_0(\eta)\right]=p\hbar_\theta N_\theta\left[\hat{f}(\eta;\ p),\hat{\theta}(\eta;\ p)\right], \tag{5.34}$$

subject to the boundary conditions:

$$\hat{f}(0;\ p)=0,\quad \hat{f}''(0;\ p)=0; \tag{5.35}$$

$$\hat{f}(1;\ p)=1,\quad \hat{f}'(1;\ p)=0; \tag{5.36}$$

$$\widehat{\theta'}(0;\ p)=1,\quad \hat{\theta}(1;\ p)=1. \tag{5.37}$$

The nonlinear operators are defined as

$$N_f\left[\hat{f}(\eta;\ p),\hat{\theta}(\eta;\ p)\right]=\ a_1\frac{\partial^4\hat{f}}{\partial\eta^4}-S\left(\frac{\partial\hat{f}}{\partial\eta}\frac{\partial^2\hat{f}}{\partial\eta^2}+\left(-\hat{f}+\eta\right)\frac{\partial^3\hat{f}}{\partial\eta^3}+3\frac{\partial^2\hat{f}}{\partial\eta^2}\right)-a_3M^2\frac{\partial^2\hat{f}}{\partial\eta^2}, \tag{5.38}$$

$$N_\theta\left[\hat{f}(\eta;\ p),\hat{\theta}(\eta;\ p)\right]=\ \frac{\partial^2\hat{\theta}}{\partial\eta^2}+Pr\left(Sa_2\left(\hat{f}-\eta\right)\frac{\partial\hat{\theta}}{\partial\eta}+Eca_4\left(4\delta^2\left(\frac{\partial\hat{f}}{\partial\eta}\right)^2+\frac{\partial^2\hat{f}^2}{\partial\eta^2}\right)\right)+a_2\theta\lambda \tag{5.39}$$

where $\hat{f}(\eta;\ p)$ and $\widehat{\theta}(\eta;\ p)$ are unknown functions with respect to $\eta$ and $p$. $\hbar_f$ and $\hbar_\theta$ are non-zero auxiliary parameters and $N_f$ and $N_\theta$ are nonlinear operators.

Also, $p\in(0,\ 1)$ is an embedding parameter. For $p=0$ and $p=1$,

$$\hat{f}(\eta;0)=f_0(\eta),\hat{f}(\eta;1)=f(\eta), \tag{5.40}$$

$$\hat{\theta}(\eta;0)=\ \theta_0(\eta),\hat{\theta}(\eta;1)=\ \theta(\eta). \tag{5.41}$$

In other words, when variation of $p$ is taken from 0 to 1 then $\hat{f}(\eta;\ p)$ and $\hat{\theta}(\eta;\ p)$ vary from $f_0(\eta)$ and $\theta_0(\eta)$ to $f(\eta)$ and $\theta(\eta)$ respectively. Taylor's series expansion of these functions yield the following:

$$\hat{f}(\eta;\ p)=f_0(\eta)+\sum_{m=1}^{\infty}f_m(\eta)p^m, \tag{5.42}$$

$$\hat{\theta}(\eta;\ p)=\theta_0(\eta)+\sum_{m=1}^{\infty}\theta_m(\eta)p^m, \tag{5.43}$$

where

$$f_m(\eta) = \frac{1}{m!}\left[\frac{\partial^m f(\eta; p)}{\partial p^m}\right]_{p=0}, \tag{5.44}$$

$$\theta_m(\eta) = \frac{1}{m!}\left[\frac{\partial^m \theta(\eta; p)}{\partial p^m}\right]_{p=0}. \tag{5.45}$$

Assuming that these nonzero auxiliary parameters are chosen so that Equations (5.42) - (5.43) converges at $p = 1$. Hence, one can obtain the following:

$$f(\eta) = f_0(\eta) + \sum_{m=1}^{\infty} f_m(\eta), \tag{5.46}$$

$$\theta(\eta) = \theta_0(\eta) + \sum_{m=1}^{\infty} \theta_m(\eta). \tag{5.47}$$

Differentiating the zeroth order deformation (5.33) – (5.34) and (5.35) – (5.37) m times with respect to $p$ and substituting $p = 0$, and finally dividing by $m!$; the m[th] order deformation $(m \geq 1)$ is

$$L_f[f_m(\eta) - \chi_m f_{m-1}(\eta)] = \hbar_f R_{f,m}(\eta), \tag{5.48}$$

$$L_\theta[\theta_m(\eta) - \chi_m \theta_{m-1}(\eta)] = \hbar_\theta R_{\theta,m}(\eta), \tag{5.49}$$

with

$$\chi_m = \begin{cases} 0, & m \leq 1 \\ 1, & m > 1 \end{cases}, \tag{5.50}$$

subject to the boundary conditions

$$f_m(0) = f_m'(0) = 0, \tag{5.51}$$

$$f_m(1) = f_m'(1) = 0, \tag{5.52}$$

$$\theta_m(0) = \theta_m(1) = 0, \tag{5.53}$$

with

$$R_{f,m}(\eta) = a_1 f_{m-1}^{iv} - S\left(\sum_{j=0}^{m-1} f_j' f_{m-1-j}'' - \sum_{j=0}^{m-1} f_j f_{m-1-j}''' + \eta f_{m-1}''' + f_{m-2}''' + 3f_{m-1}''\right)$$
$$-a_3 M^2 f_{m-1}'' \tag{5.54}$$

$$R_{\theta,m}(\eta) = \theta_{m-1}'' + Pr\left(Sa_2\left(\sum_{j=0}^{m-1} f_j \theta_{m-1-j}' - \eta\theta_{m-1}' - \theta_{m-2}'\right) +\right.$$
$$\left. Eca_4\left(4\delta^2 \sum_{j=0}^{m-1} f_j' f_{m-1-j}' + \sum_{j=0}^{m-1} f_j'' f_{m-1-j}''\right)\right) + a_2\lambda\theta_{m-1} \tag{5.55}$$

Solving the corresponding m[th] order deformation equations,

$$f_m(\eta) = f_m^*(\eta) + C_1 + C_2\,\eta + C_3\eta^2 + C_4\eta^3 \tag{5.56}$$

$$\theta_m(\eta) = \theta_m^*(\eta) + C_5 + C_6\eta \tag{5.57}$$

Here $f_m^*$ and $\theta_m^*$ are given by particular solutions of the corresponding m[th] order equations and the constants $C_i(\ i = 1,2,\ldots,6)$ are to be determined by the boundary conditions.

### 5.4.1 Convergence of solution

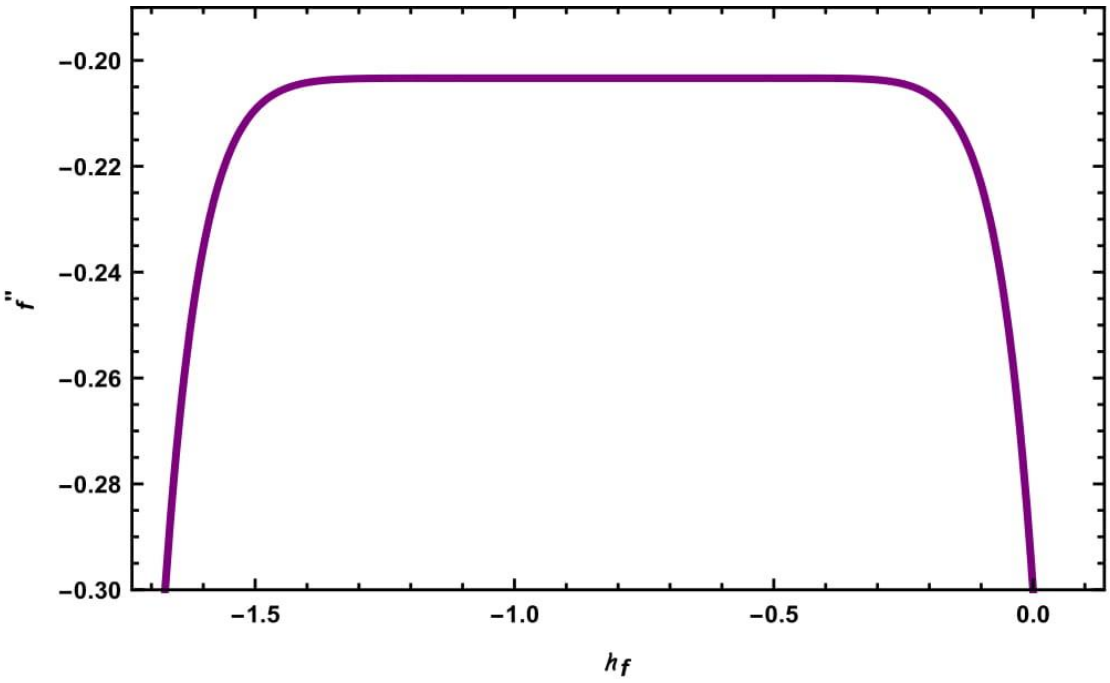


**Figure 5.2:** H-Curve of $f''(0)$ for different values of $\hbar_f$ at $\phi = 0.03,\ M = 0.6,$ $Nr = 0.6,\ Pr = 7.0,\ S = 0.9,\ Ec = 0.02,\ \delta = 0.02\ and\ \lambda = 1.4.$

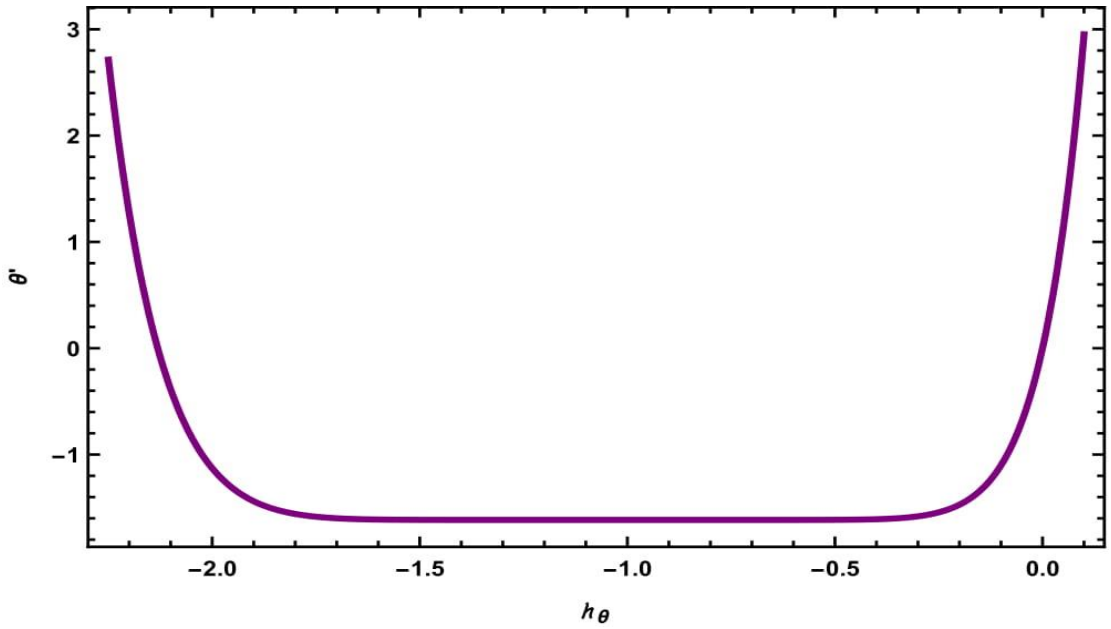


**Figure 5.3:** H-Curve of $\theta'(0)$ for different values of $\hbar_\theta$ at $\phi = 0.03,\ M = 0.6,$ $Nr = 0.6, Pr = 7.0,\ S = 0.9,\ Ec = 0.02,\ \delta = 0.02\ and\ \lambda = 1.4.$

Convergence of the HAM solutions and their rate of approximations strongly depend on the values of the auxiliary parameters $\hbar_f$ and $\hbar_\theta$. For this purpose the associated h-curves are plotted in Figures 5.2 – 5.3. The Figure 5.2 and Figure 5.3 clearly suggest admissible ranges for the auxiliary parameters.

## 5.5 Results and Discussion

Solutions are obtained using appropriate codes in Mathematica. Obtained results are explained with the help of graphs. Parametric study is performed for Squeeze number $S$, magnetic parameter $M$, Nanoparticle volume fraction $\emptyset$, Eckert number $Ec$, Prandtl number $Pr$ and Heat generation/absorption parameter $\delta$ in Figures 5.4 – 5.19.

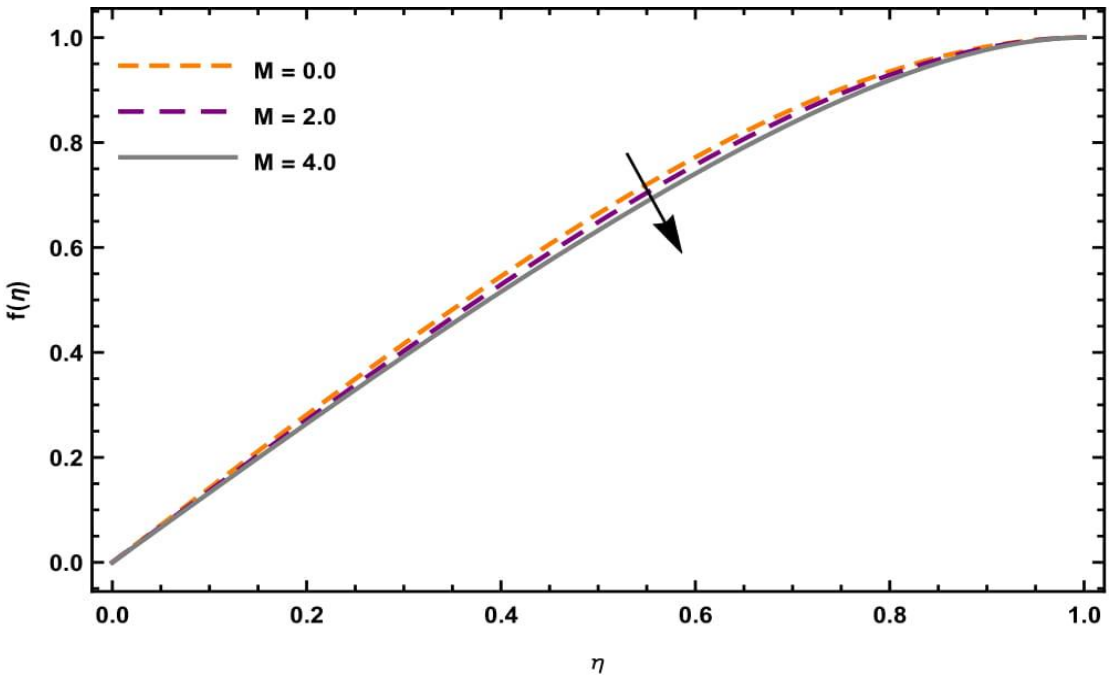


**Figure 5.4**: Velocity profile $f$ for different values of $\eta$ and $M$ at $S = 0.9,\ Nr = 0.6,$ $Pr = 7.0,\ \phi = 0.03,\ Ec = 0.02,\ \delta = 0.02\ and\ \lambda = 1.4.$

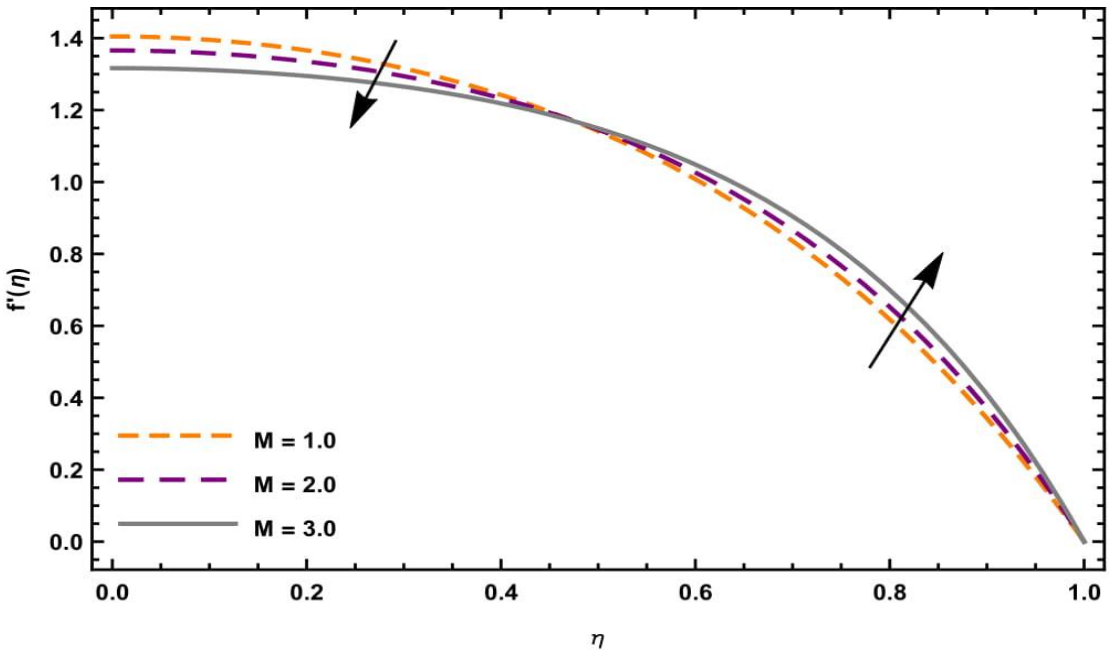


**Figure 5.5:** Velocity profile $f'$ for different values of $\eta$ and $M$ at $S = 0.9,\ Nr = 0.6,$ $Pr = 7.0,\ \phi = 0.03,\ Ec = 0.02,\ \delta = 0.02\ and\ \lambda = 1.4.$

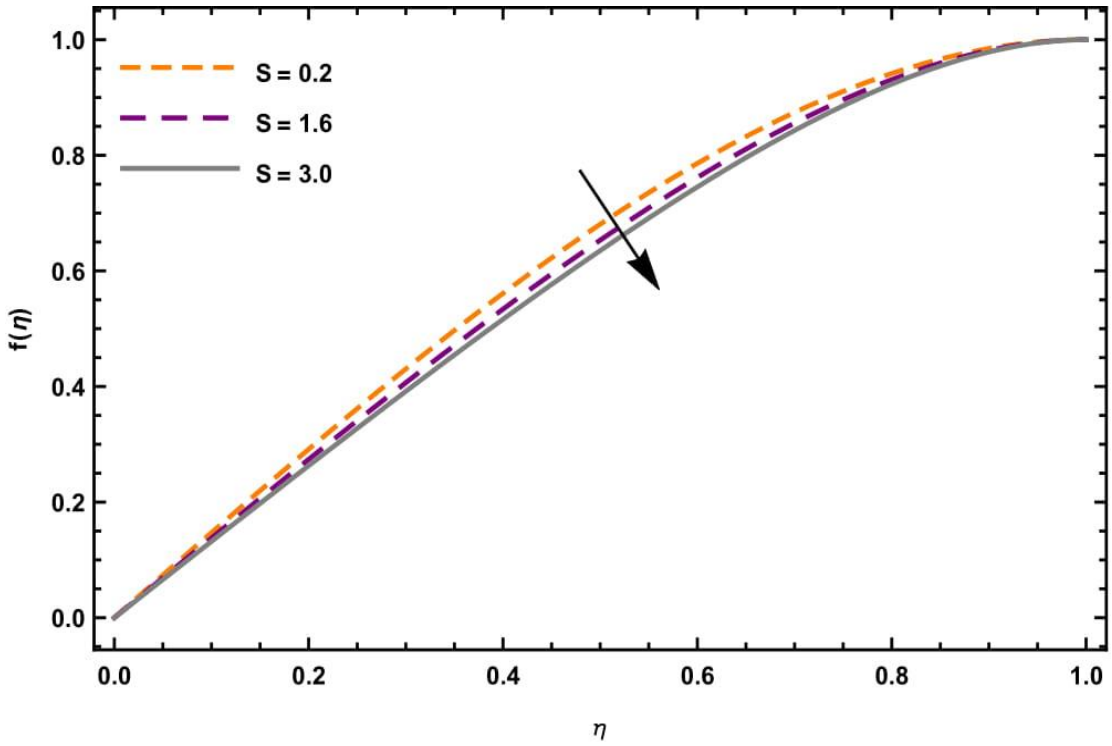


**Figure 5.6:** Velocity profile $f$ for different values of $\eta$ and $S$ at $M = 0.6,\ Nr = 0.6,$ $Pr = 7.0,\ \phi = 0.03,\ Ec = 0.02,\ \delta = 0.02\ and\ \lambda = 1.4.$

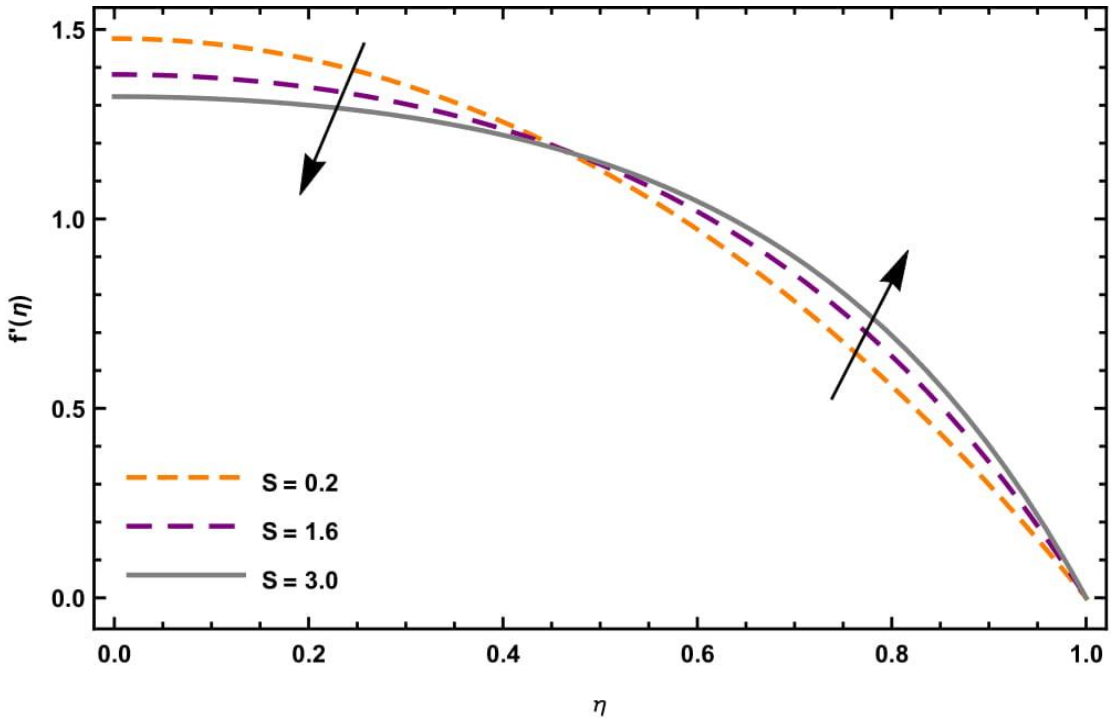


**Figure 5.7:** Velocity profile $f'$ for different values of $\eta$ and $S$ at $M = 0.6,\ Nr = 0.6,$ $Pr = 7.0,\ \phi = 0.03,\ Ec = 0.02,\ \delta = 0.02\ and\ \lambda = 1.4.$

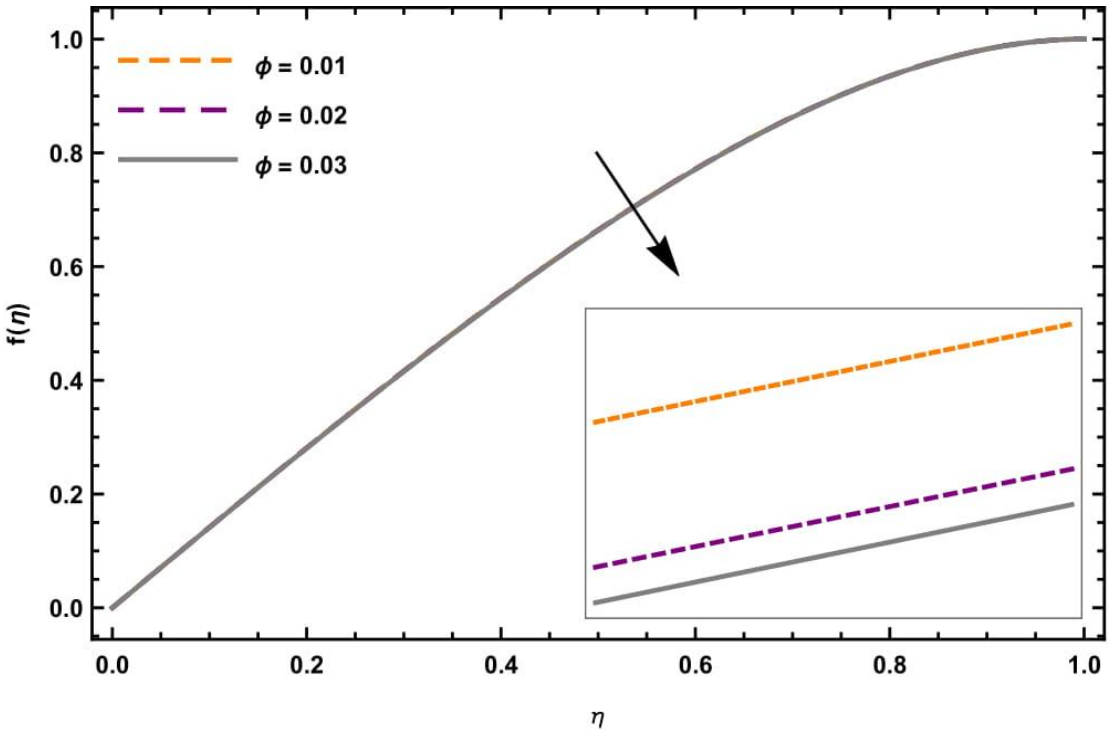


**Figure 5.8:** Velocity profile $f$ for different values of $\eta$ and $\phi$ at $M = 0.6$, $Nr = 0.6, Pr = 7.0,\ S = 0.9,\ Ec = 0.02,\ \delta = 0.02$ *and* $\lambda = 1.4$.

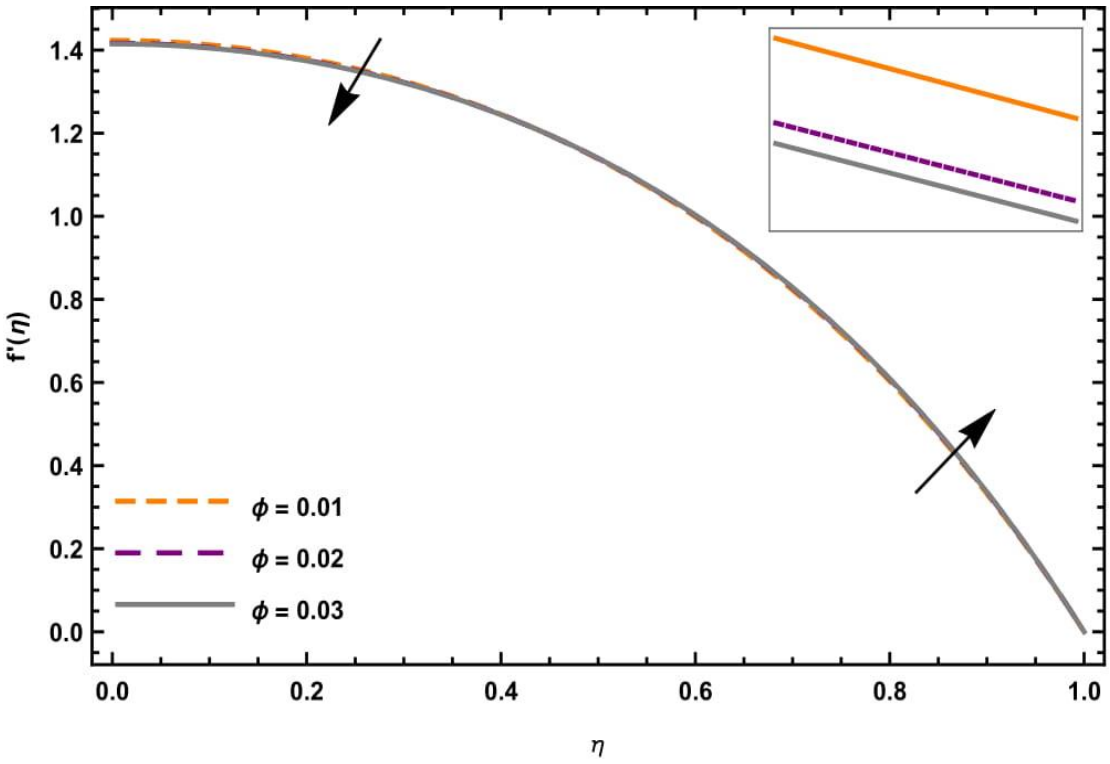


**Figure 5.9:** Velocity profile $f'$ for different values of $\eta$ and $\phi$ at $M = 0.6$, $Nr = 0.6, Pr = 7.0,\ S = 0.9,\ Ec = 0.02,\ \delta = 0.02$ *and* $\lambda = 1.4$.

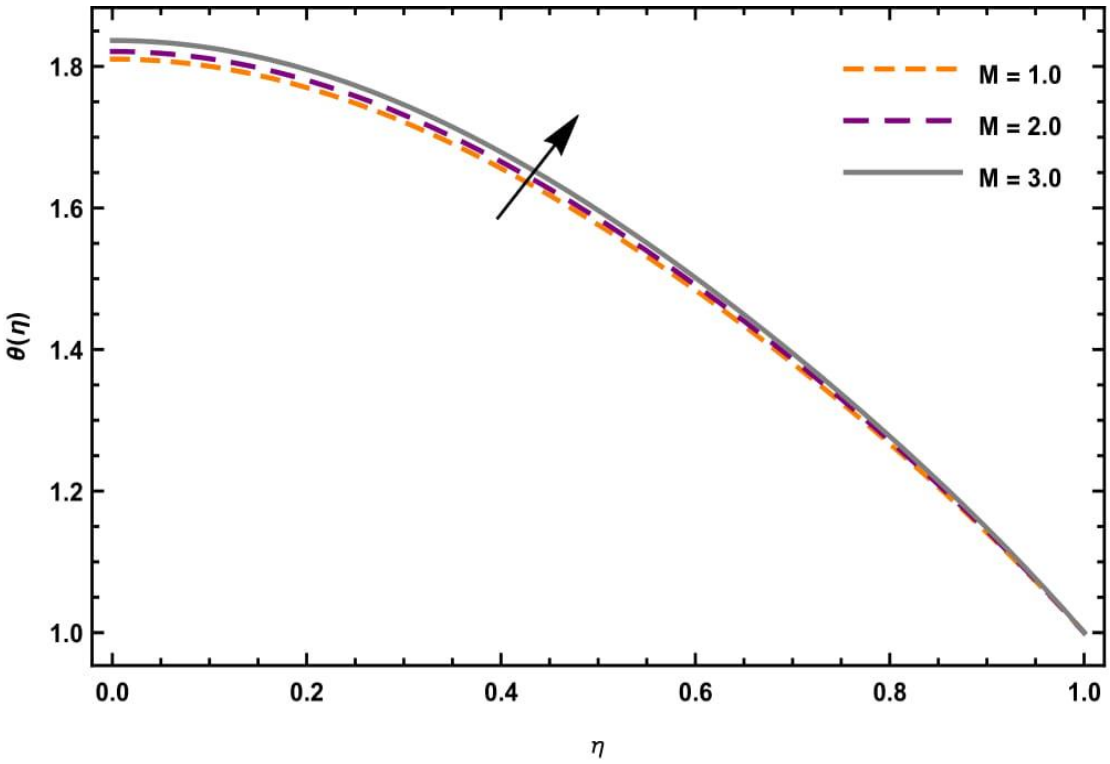


**Figure 5.10:** Temperature profile $\theta$ for different values of $\eta$ and M at $S = 0.9$, $Nr = 0.6,\ Pr = 7.0,\ \phi = 0.03,\ Ec = 0.02,\ \delta = 0.02\ and\ \lambda = 1.4$.

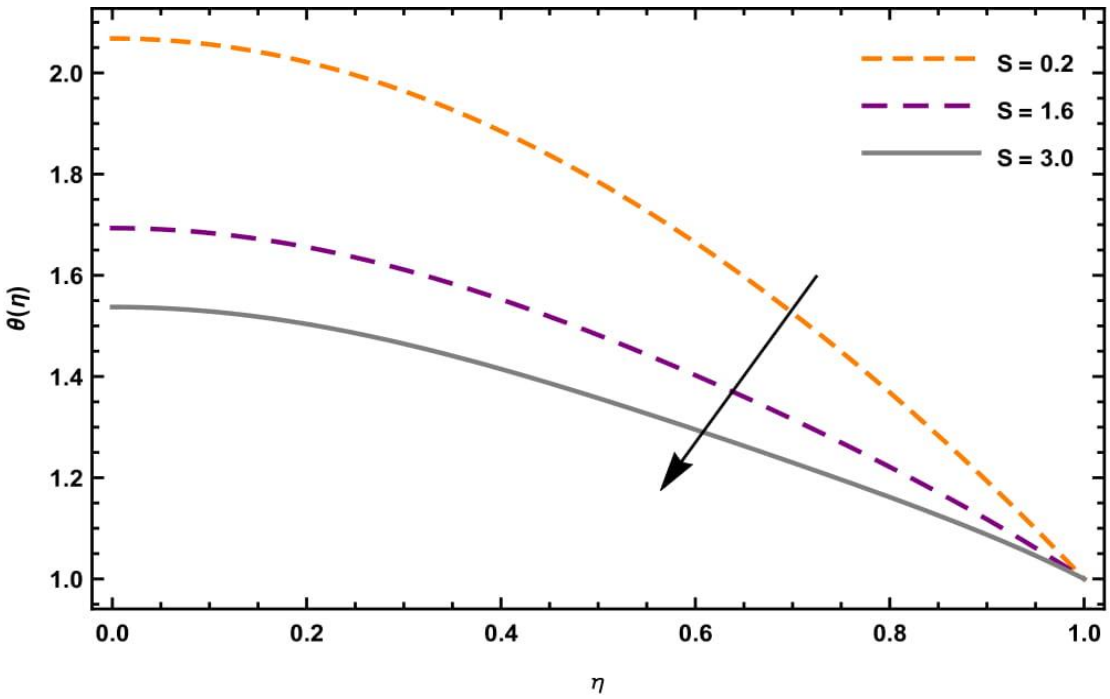


**Figure 5.11:** Temperature profile $\theta$ for different values of $\eta$ and $S\ \ M = 0.6$, $Nr = 0.6, Pr = 7.0, \phi = 0.03,\ Ec = 0.02,\ \delta = 0.02\ and\ \lambda = 1.4$.

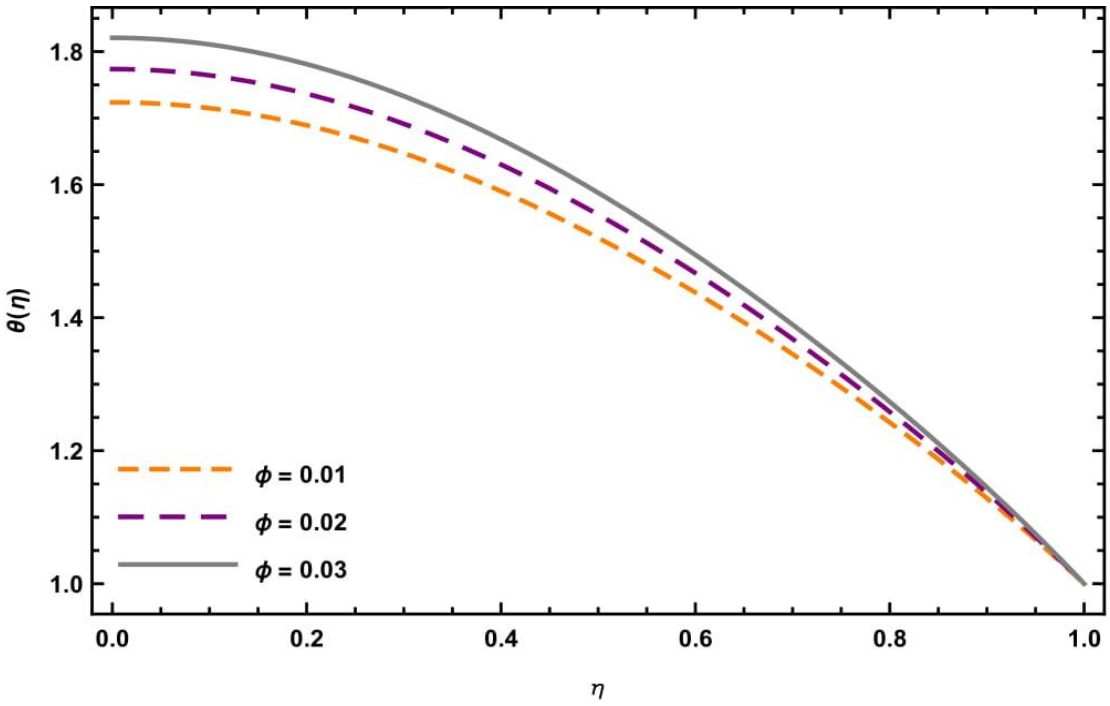


**Figure 5.12:** Temperature profile $\theta$ for different values of $\eta$ and $\phi$ at $M = 0.6$, $Nr = 0.6$, $Pr = 7.0$, $S = 0.9$, $Ec = 0.02$, $\delta = 0.02$ *and* $\lambda = 1.4$.

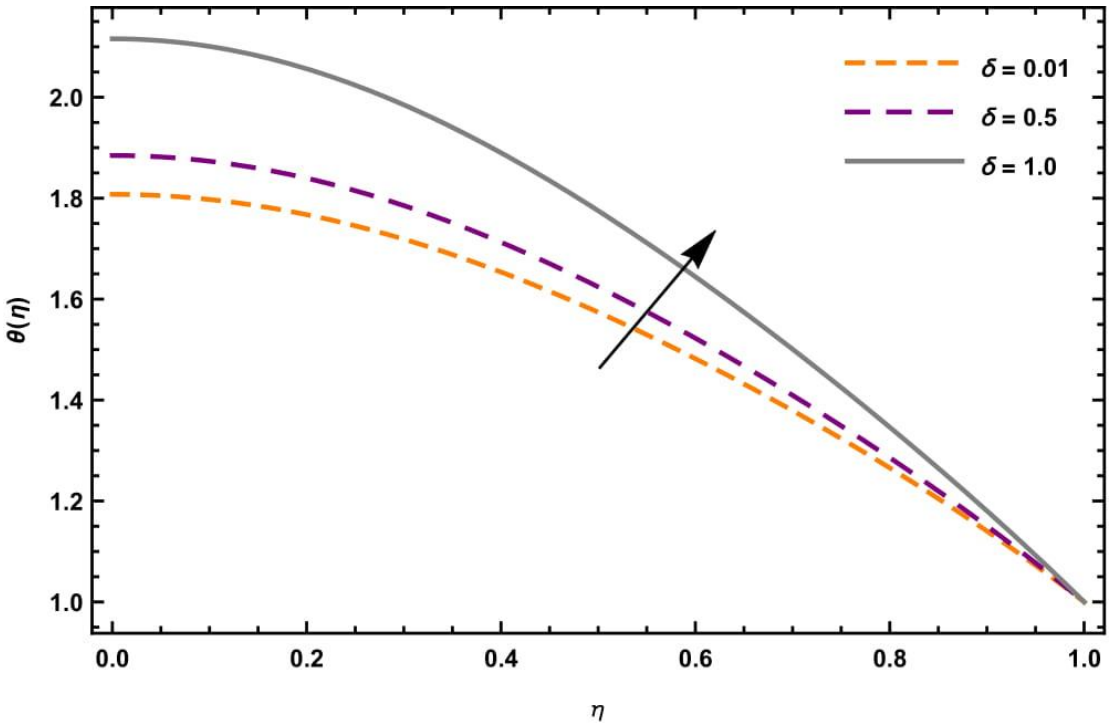


**Figure 5.13:** Temperature profile $\theta$ for different values of $\eta$ and $\delta$ at $S = 0.9$, $Nr = 0.6$, $M = 0.6$, $\phi = 0.03$, $Ec = 0.02$, $Pr = 7.0$ *and* $\lambda = 1.4$.

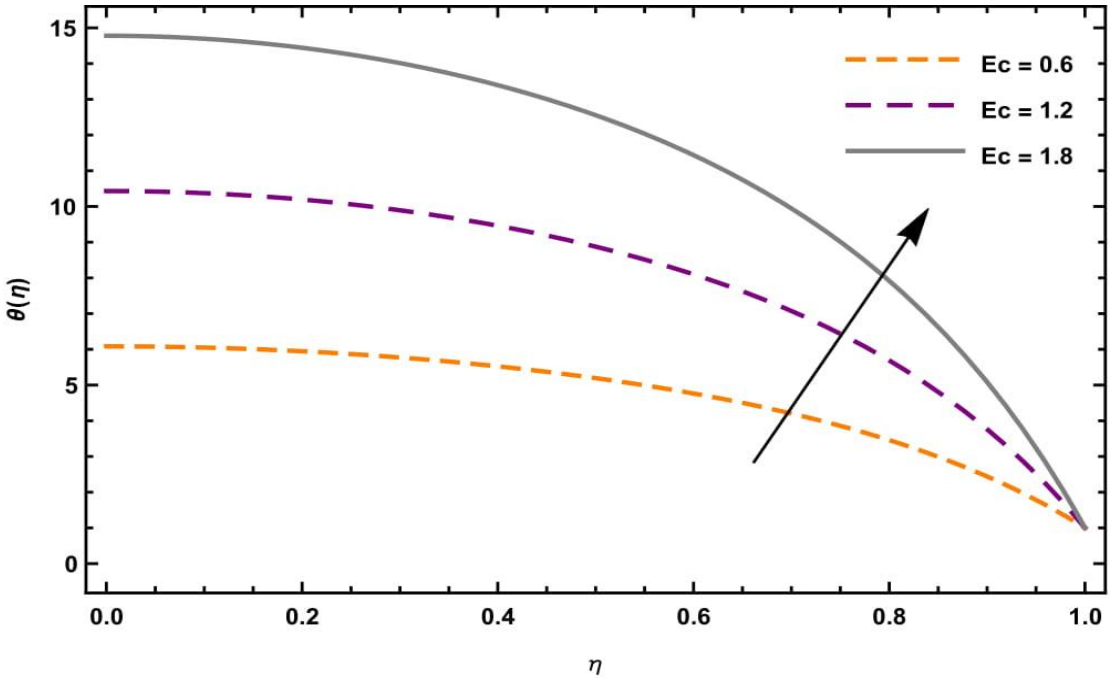


**Figure 5.14:** Temperature profile $\theta$ for different values of $\eta$ and Ec at $S = 0.9$, $Nr = 0.6$, $M = 0.6$, $\phi = 0.03$, $\delta = 0.02$, $Pr = 7.0$ *and* $\lambda = 1.4$.

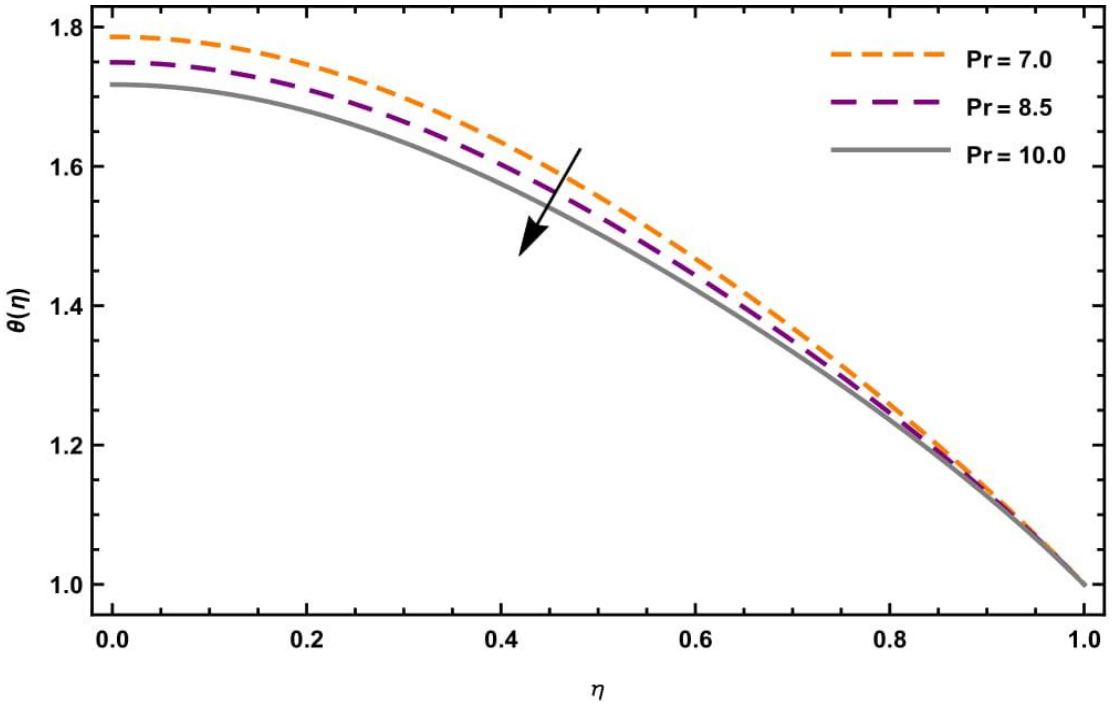


**Figure 5.15:** Temperature profile $\theta$ for different values of $\eta$ and $Pr$ at $S = 0.9$, $Nr = 0.6, M = 0.6$, $\phi = 0.03$, $Ec = 0.02$, $\delta = 0.02$ *and* $\lambda = 1.4$.

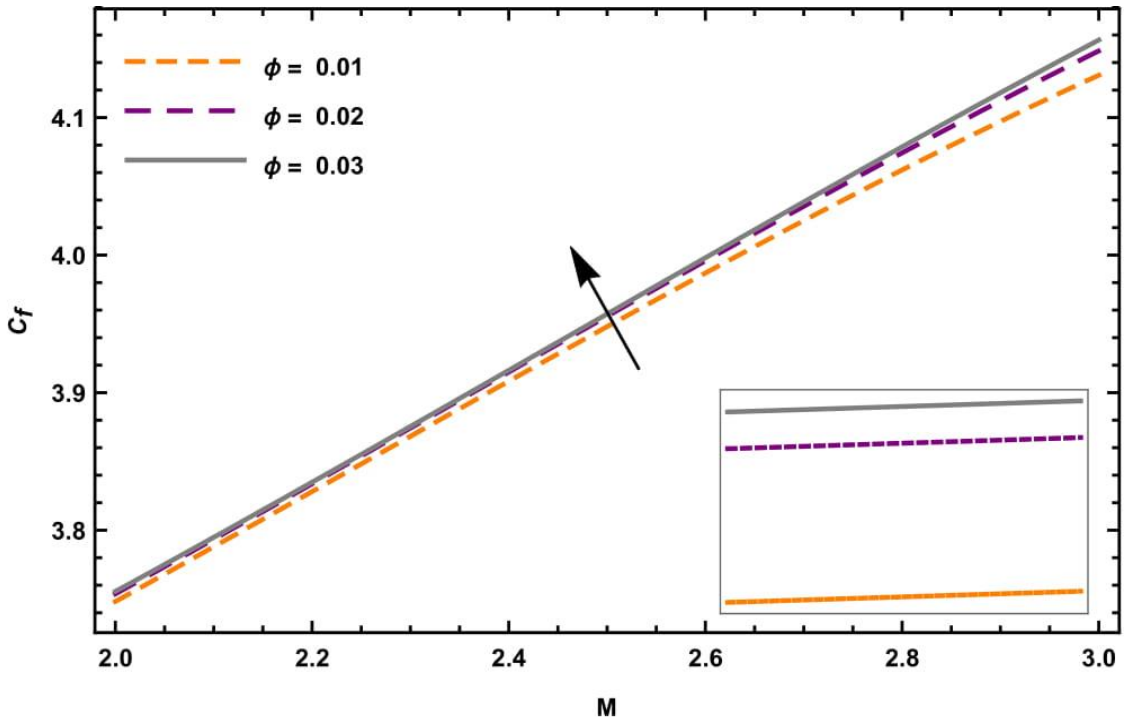


**Figure 5.16:** Effect of magnetic parameter M and $\phi$ on Skin friction coefficient at $Nr = 1.8,\ Pr = 6.2,\ S = 0.9,\ Ec = 1.1,\ \delta = 0.1\ and\ \lambda = 1.4.$

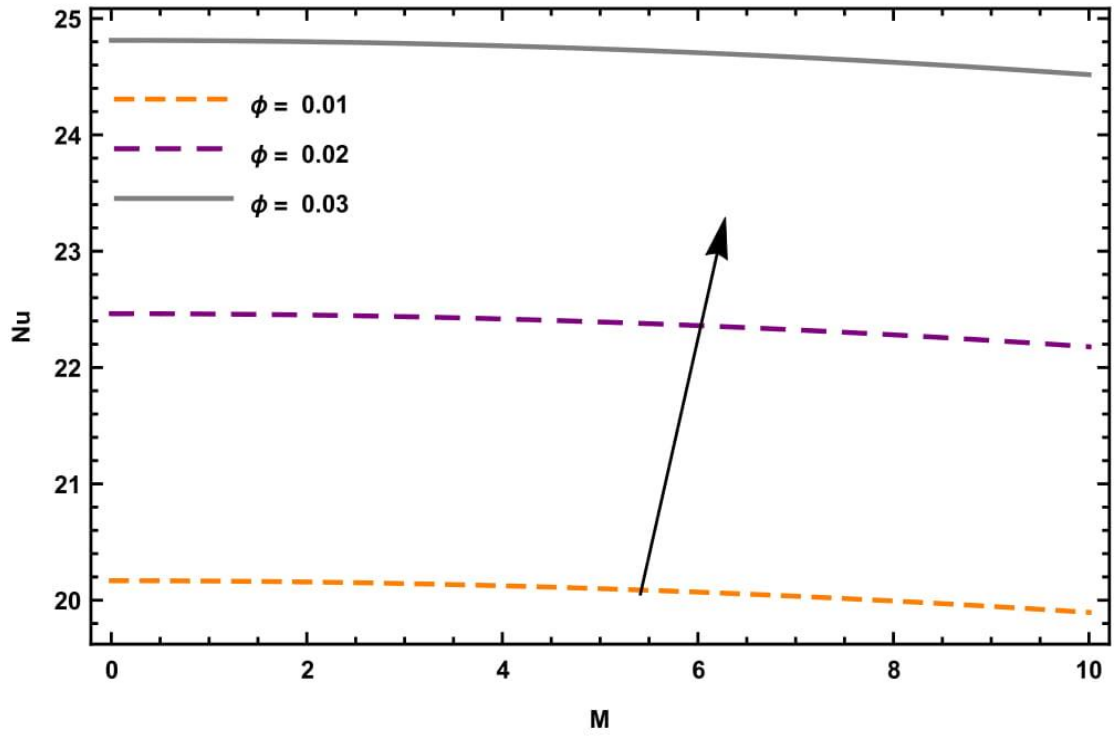


**Figure 5.17:** Effect of magnetic parameter M and $\phi$ on Nusselt Number at $Nr = 1.8,\ Pr = 6.2, S = 0.9,\ Ec = 1.1,\ \delta = 0.1\ and\ \lambda = 1.4.$

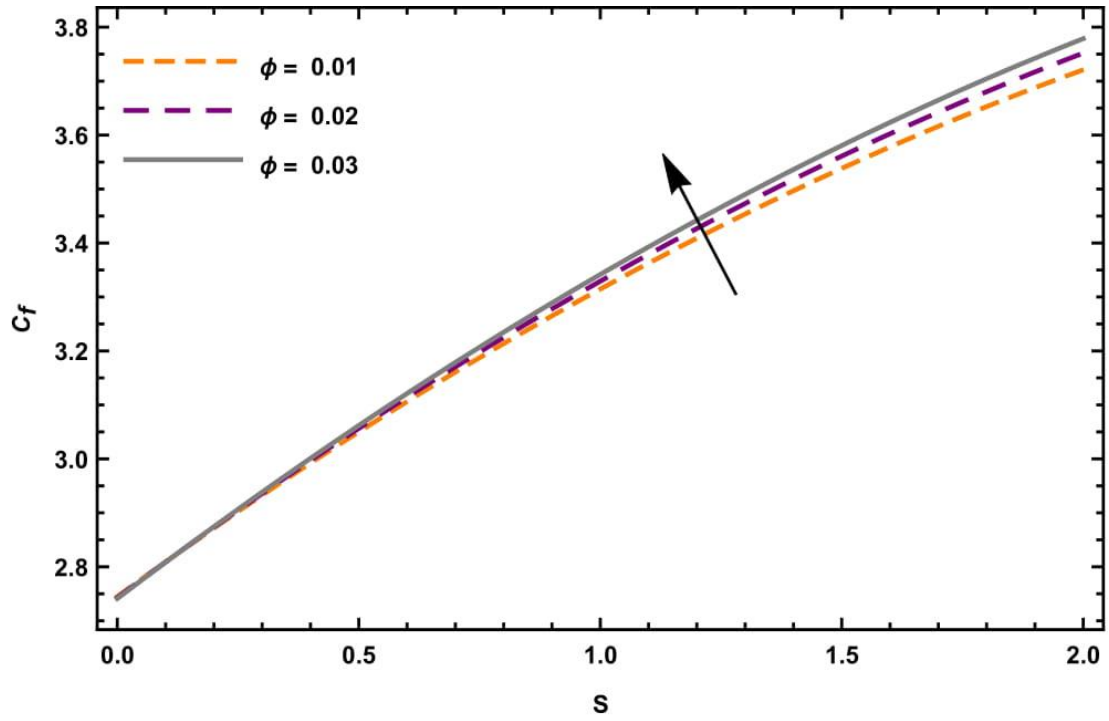


**Figure 5.18:** Effect of Squeezing parameter S and $\phi$ on Skin friction coefficient at $Nr = 1.8,\ Pr = 6.2,\ M = 0.6,\ Ec = 1.1,\ \delta = 0.1\ and\ \lambda = 1.4$.

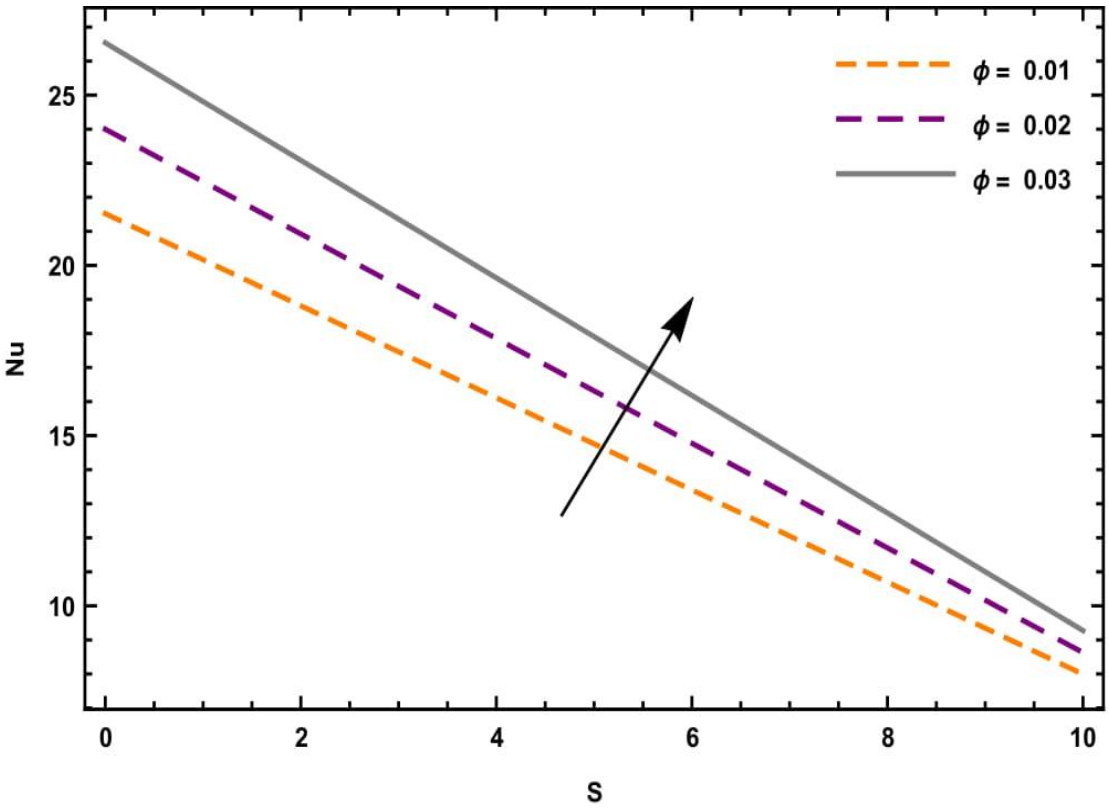


**Figure 5.19:** Effect of Squeezing parameter S and $\phi$ on Nusselt Number at $M = 0.6,\ Pr = 6.2, Nr = 1.8,\ Ec = 1.1,\ \delta = 0.1\ and\ \lambda = 1.4$.

It is apparent from Figures 5.4 – 5.5 that magnetic field limits flow. This is owing to the Lorentz force resulting from variation of $M$. Figures 5.6 – 5.7 illustrate role of $S$ on fluid flow. It shows that velocity decreases when $S$ is increased. Figures 5.8 – 5.9 show that velocity can be increased by decreasing $\emptyset$. Figure 5.10 shows that there is increase in temperature with $M$. It is observed from Figure 5.11 that there is decrease in temperature with increase in $S$. It is marked from Figure 5.12 that temperature accelerates with nanoparticle volume fraction $\phi$. It is noticed from Figure 5.13 that the fluid temperature is escalating with heat generation/absorption parameter $\delta$. Figure 5.14 depicts that temperature increases with increasing values of $Ec$. Negative impact of $Pr$ on temperature profile is evident from Figure 5.15. It is obvious as thermal conductivity of the nanofluid reduces with $Pr$.

Effects of $M$, $S$ and $\emptyset$ on skin friction and Nusselt number can be found in Figures 5.16 – 5.19. It is evident that both Skin friction and Nusselt number increase with increase in nanoparticle volume fraction.

## 5.6 Conclusion

The most important concluding remarks can be summarized as follows:

- Nanofluid velocity decays with surge in $\emptyset$ and $M$.
- Nanofluid temperature can be amplified by accumulative $\emptyset$ or $Ec$.
- Nanofluid temperature tends to decrease with rising values of $Pr$.
- Skin friction can be minimized by decreasing $\emptyset$.
- Nusselt number surges with $\emptyset$.